Modifications in Coordination Structure of Mg[TFSA]2-Based Supporting Salts for High-Voltage Magnesium Rechargeable Batteries

Journal:	*Physical Chemistry Chemical Physics*
Manuscript ID	CP-ART-03-2019-001400.R2
Article Type:	Paper
Date Submitted by the Author:	11-Apr-2019
Complete List of Authors:	MANDAI, Toshihiko; Iwate Daigaku, mandai@iwate-u.ac.jp; National Institute for Materials Science, Global Research Center for Environment and Energy based on Nanomaterials Science; National Institute for Materials Science Tatesaka, Kenji; Iwate Daigaku, Department of Chemistry and Biological Sciences Soh, Kenya; Tokyo Metropolitan University, Department of Applied Chemistry Masu, Hyuma; Chiba University, Chemical Analysis Center; TokushimaBunriUniversity, Choudhary, Ashu; National Institute for Materials Science, Center for Materials Research by Information Integration Tateyama, Yoshitaka; National Institute for Materials Science, Global Research Center for Environment and Energy based on Nanomaterials Science; National Institute for Materials Science, Center for Materials Research by Information Integration, Research and Services Division of Materials Data and Integrated System Ise, Ryuta; Keio University, Applied Chemistry Imai, Hiroaki; Keio University, Applied Chemistry Takeguchi, Tatsuya; Iwate Daigaku, Chemsitry and Biological Sciences Kanamura, Kiyoshi; Tokyo metropolitan university,

Physical Chemistry Chemical Physics

Modifications in Coordination Structure of $Mg[TFSA]_2$-Based Supporting Salts for High-Voltage Magnesium Rechargeable Batteries

Toshihiko Mandai,[1,2,§,] Kenji Tatesaka,[1] Kenya Soh,[3] Hyuma Masu,[4] Ashu Choudhary,[5] Yoshitaka Tateyama,[2,5] Ryuta Ise,[6] Hiroaki Imai,[6] Tatsuya Takeguchi,[1] and Kiyoshi Kanamura[3]*

[1]Department of Chemistry and Biological Sciences, Faculty of Science and Engineering, Iwate University, Ueda 4-3-5, Morioka 020-8551, Japan

[2]Global Research Center for Environment and Energy based on Nanomaterials Science (GREEN), National Institute for Materials Science (NIMS), 1-1 Namiki, Tsukuba, Ibaraki 305-0044, Japan

[3]Department of Applied Chemistry, Tokyo Metropolitan University, 1-1 Minami-Osawa, Hachioji, Tokyo 192-0397, Japan

[4]Center for Analytical Instrumentation, Chiba University, 1-33 Yayoi-cho, Inage-ku, Chiba 263-8522, Japan

[5]Center for Materials Research by Information Integration (CMI2), Research and Services Division of Materials Data and Integrated System (MaDIS), National Institute for Materials Science (NIMS), 1-2-1 Sengen, Tsukuba, Ibaraki, 305-0047, Japan

[6]Department of Applied Chemistry, Faculty of Science and Technology, Keio University, 3-14-1 Hiyoshi, Kohoku-ku, Yokohama 223-8522, Japan

[§]Present address: Research Center for Energy and Environmental Materials, National Institute for Materials Science (NIMS), 1-1 Namiki, Tsukuba, Ibaraki 305-0044, Japan

CORRESPONDING AUTHOR FOOTNOTES

Telephone: +81-29-860-4464, E-mail: MANDAI.Toshihiko@nims.go.jp

Abstract

To achieve a sustainable-energy society in the future, next-generation highly efficient energy storage technologies, particularly those based on multivalent metal negative electrodes, are urgently required to be developed. Magnesium rechargeable batteries (MRBs) are promising options owing to the many advantageous chemical and electrochemical properties of magnesium. However, the substantially low working voltage of sulfur-based positive electrodes may hinder MRBs in becoming alternatives to current Li-ion batteries. We proposed halide-free noncorrosive ionic liquid-based electrolytes incorporating $Mg[TFSA]_2$ for high-voltage MRB applications. Upon the complexation of $Mg[TFSA]_2$ with tetraglyme (G4) and strict control of the liquid states, the electrolytes achieved excellent anodic stability up to 4.1 V *vs*. Mg^{2+}/Mg even at 100 ºC. The modest electrochemical activities for magnesium deposition/dissolution in the $[Mg(G4)][TFSA]_2$/ionic liquid electrolyte can be improved by certain modifications to the coordination state of $[TFSA]^-$. Dialkyl sulfone was found to be effective in changing the coordination state of $[TFSA]^-$ from associated to isolated (free). This coordination change successfully promoted magnesium deposition/dissolution reactions, particularly in the coexistence of ether ligand. By contrast, the coordination of Mg^{2+} by strongly donating agents such as dimethyl sulfoxide and alkylimidazole led to the complexes inactive electrochemically, suggesting that interaction between Mg^{2+} and coordination agents predominates the fundamental electrochemical activity. We also demonstrated that an enhancement in the electrochemical activity of electrolytes contributed to improvements in the cycling ability of magnesium batteries with 2.5 V-class $MgMn_2O_4$ positive electrodes.

Introduction

Energy storage technologies have evolved from lithium-ion batteries to rechargeable batteries based on multivalent metal negative electrodes; these have recently attracted significant interest. The non-aqueous magnesium rechargeable battery (MRB) is a promising candidate for next-generation energy storage options because magnesium exhibits several beneficial properties over its lithium counterpart. These properties include a large volumetric capacity, large natural abundance, and the resulting cost effectiveness.[1–7] MRBs also offer improved safety owing to their nontoxic properties and absence of dendrite growth during the electrodeposition of magnesium.[8]

Chevrel-phase Mo_6S_8 has been recognized as the representative positive electrode active material for MRBs owing to its successful charge–discharge cycle under various experimental conditions.[9–11] The substantially low working voltage at *ca*. 1.0 V and low deliverable capacity (up to 122 mAh g^{-1}) may hinder the materialization of practical MRBs that can replace current lithium-ion battery technologies. Some researchers focused on the use of elemental sulfur as a high-capacity active material, and significant progress for Mg–S batteries has been accomplished in recent years.[6,7,12–17] Unfortunately, the sluggish electrochemical activity and poor reaction kinetics of sulfur with Mg^{2+} and large volume changes associated with the charge–discharge cycle of the Mg–S batteries are major obstacles to practical realization.[18] Another option for the positive electrode is utilizing transition metal oxides with high Mg^{2+} redox potential. A somewhat reversible intercalation/de-intercalation of Mg^{2+} into/from several transition metal oxides, MgM_2O_4, M_2O_4 and MO_2 (M = Co, Mn, Fe), was demonstrated experimentally.[19–22] Such achievements have opened the possibility of high-voltage (HV) MRB realization; however, there are very limited examples of true “magnesium metal” batteries

owing to a lack of suitable electrolyte materials that support reversible magnesium deposition/dissolution and sufficient stability.

Research into novel concepts in designing electrodes and electrolytes for MRBs has progressed significantly in the last few years. As the intercalation-type positive electrodes suffer from poor battery performance due to strong binding of Mg^{2+} ions by the host matrix, conversion-type electrodes are rather promising.[6,7] The remarkable advancements for the specific capacity and long-term cycling stability have been accomplished by using the nanostructured CuS,[23–26] while its redox potential is still insufficient. For MRB electrolytes, magnesium salts with weakly coordinated anions, such as carborane,[27–30] fluoroalkoxyborate,[13,16,31] and fluoroalkoxyaluminate,[32,33] are potential candidates owing to their high oxidative stability and good compatibility with the magnesium metal. Current state-of-the-art MRB technology is, however, not suitable for practical battery applications mainly due to the commercial unavailability of the candidate materials, the production costs, and non-trivial special experimental techniques and set-up.

Regarding thermal and anodic stabilities and commercial availability, magnesium bis(trifluoromethanesulfonyl)amide ($Mg[TFSA]_2$) is a promising supporting salt for HV MRBs; a previous theoretical study suggested that oxide-based positive-electrode active materials not only require high anodic stability but also high operation temperatures owing to large migration barriers in the oxide-based lattice.[6,34] Since the first systematic studies,[35] several researchers have studied $Mg[TFSA]_2$-based electrolytes with respect to fundamental Mg^{2+} coordination structures and structural-electrochemical properties and relationships. To achieve sufficient thermal stability, ionic liquids (ILs) are regarded as the first option for thermally stable solvents. The electrochemical activity

of IL-based electrolytes containing $Mg[TFSA]_2$ is, however, still controversial.[36] The coordination structure of Mg^{2+} in electrolyte solutions likely plays a key role in electrochemical activity, as electrolyte solutions of $Mg[TFSA]_2$ dissolved in hybrid IL-glyme solvents have showed reasonable magnesium redox activity.[37–39] Unfortunately, the uncoordinated free glymes and/or dehydration agents in such hybrid electrolyte solutions determine the anodic limits of the electrolytes.

In this study, we propose the rational design of IL-based electrolytes by incorporating modified $Mg[TFSA]_2$-based supporting salts applicable to HV MRBs. Pyrrolidinium-based ILs were selected for this purpose because of their superior electrochemical stability compared to imidazolium-based counterparts.[40,41] After appropriate modifications to the coordination structure and solution states, the resulting electrolytes showed excellent thermal and electrochemical stability with electrochemical activity for magnesium deposition/dissolution. Such high stability and low coordinating ability achieved by the ILs enable the electrolytes to be compatible with HV MRBs, while typical hybrid IL-glyme electrolytes suffer from oxidative decomposition and undesired anodic dissolution of the active materials during charging. The design concept for more efficient $Mg[TFSA]_2$-based electrolyte materials is reported.

Experimental

Materials

Battery-grade magnesium bis(trifluoromethanesulfonyl)amide ($Mg[TFSA]_2$), magnesium chloride ($MgCl_2$), and tetraglyme (G4) were purchased from Kishida Chemical Co., Ltd. Anhydrous dimethylsulfoxide (DMSO) was obtained from Sigma-Aldrich. Grignard reagent (*ca*. 2 mol dm^{-3}

C_2H_5MgCl in THF), silver nitrate ($AgNO_3$), *N*-methylimidazole (MIm), *N*-ethylimidazole (EIm), ethyl methyl sulfone ($EMSO_2$), ethyl propyl sulfone ($EPSO_2$), dipropyl sulfone ($DPSO_2$), 3-methylsulfolane (3-MeSL), *N*-methyl-*N*-propylpyrrolidinium bis(trifluoromethanesulfonyl)amide ($[PYR_{13}][TFSA]$), *N*-butyl-*N*-methylpyrrolidinium ($[PYR_{14}]^+$) paired with [TFSA], bis(fluorosulfonyl)amide [FSA], bis(pentafluoroethanesulfonyl)amide [BETA], and dicynaoamide [DCA] were all purchased from Tokyo Chemical Industry Co., Ltd. Maglution™ B01 was purchased from Wako Chemical. Triglyme (G3; for electrochemistry) and dimethoxyethane (DME) were obtained from Kanto Chemical Co., Inc. *N*-alkylimidazoles (RIm) were purified by vacuum distillation prior to use.

$Mg[TFSA]_2$ and all ILs were dried under vacuum heating at 120 ºC for several days and stored in an Ar-filled glovebox before use. The Grignard reagent and ILs were mixed in a 1:1 volume ratio for a preliminary survey. The $Mg[TFSA]_2$-based IL electrolyte solutions were prepared by mixing prefixed amounts of $Mg[TFSA]_2$ and various ligands in $[PYR_{13}][TFSA]$, followed by vigorous stirring at 100 ºC for several days in the glovebox (<1 ppm H_2O, 1 ppm < O_2). For the electrolytes with the Cl-based additive, the molar ratio between Mg and Cl was fixed at 1:1.5. It is well known that the water contamination in electrolytes has a significant impact on the electrochemical properties.[42,43] The water content of the prepared electrolytes was measured by Karl Fischer titration, and it was less than 50 ppm.

The positive electrode active materials for magnesium batteries, $MgCo_2O_4$ and $MgMn_2O_4$, were synthesized by an inverse co-precipitation method according to a procedure reported by another study.[22] The aqueous magnesium and cobalt or manganese nitrate solutions prepared by dissolving 0.08 M $Mg(NO_3)_2$ and 0.16 M $Co(NO_3)_2$ or $Mn(NO_3)_2$ in deionized water, respectively, were added

to a sodium carbonate aqueous solution dropwise under vigorous stirring at 80 ºC. The resulting suspension was filtered, and then the collected products (precursors) were washed with deionized water to remove Na-containing by-products. The precursors were air-dried at 80 ºC for 24 h, followed by calcination under an air atmosphere at 500 ºC for 24 h, resulting in the desired product of $MgCo_2O_4$ and $MgMn_2O_4$ as a black powder.

Measurements

Cyclic voltammetry (CV), linear sweep voltammetry (LSV), chronoamperometry (CA), and galvanostatic charge–discharge measurements were conducted with a three-electrode beaker cell. For CV and CA measurements, a Pt disk and a magnesium ribbon (Wako Pure Chemical) served as a working and counter electrode, respectively. To suppress kinetic passivation reactions between deposited magnesium and electrolytes,[44] the CV measurements for chloride-free electrolytes were performed at relatively higher scan rate of 50 mV s^{-1}. The LSV measurements were performed on Pt, Al (99.99%, nilaco), and stainless steel (SS, SUS304) working electrodes with a fixed exposed area of 0.3 cm^2 at 100 ºC, with a scan rate of 1 mV s^{-1} to evaluate the quasi-static electrochemical stability. Aiming at future practical materialization of MRBs, the stability of non-noble metal working electrodes (Al and SS) toward the present electrolytes were also studied. A reference electrode fabricated by soaking Ag wire in (0.01 mol dm^{-3} $AgNO_3$ + 0.1 mol dm^{-3} $Mg[TFSA]_2$)/G3 solution, confined in a glass tube with a liquid junction of a porous Vycor glass, was employed for all electrochemical measurements. The electrode potential of the reference electrode was calibrated using a solution of C_2H_5MgCl-$AlCl_3$/THF to be −2.62 V *vs*. the reference, which corresponds to 0 V *vs*. Mg^{2+}/Mg^0.[45] All electrochemical cells were assembled in the glovebox. The CV, LSV, and CA

measurements were conducted using an electrochemical analyzer HSV-110 (Hokuto) or VSP (Bio-Logic). All electrochemical measurements were conducted at least three times, and the results were confirmed to be reproducible.

The surfaces of the Pt working and magnesium counter electrodes were observed with scanning electron microscopy (SEM; JSM-6490A, JEOL) and subsequently characterized by energy dispersive X-ray spectroscopy (EDX) and X-ray photoelectron spectroscopy (XPS; VersaProbe 5000 ULVAC-PHI spectrometer). After soaking a magnesium ribbon in each IL for 24 h at 100 ºC, the ribbon was washed with anhydrous DME to remove the residual electrolyte and then placed in an airtight chamber and transferred for EDX or XPS analysis without any exposure to air. XPS measurements were performed with an Al Kα X-ray source under a base pressure of 6.7×10^{-8} Pa. The binding energy was calibrated using the C1s peak from sp2-hybridized carbon at 284.5 eV as a reference.

Raman spectra of a series of electrolyte solutions and their ingredients were collected with a laser Raman spectrometer NRS1000 (JASCO) or Raman microscope (Horiba) equipped with a 532-nm laser at a resolution of 4 cm^{-1}. The spectra were recorded in the range of 100–1500 cm^{-1} at 22±2 °C. The samples were sealed in a glass tube under an Ar atmosphere in the glovebox and transferred to the Raman setup without exposure to air. For the colored samples, the Raman spectra were collected with a Nicolet iS50R FT-Raman spectrometer (Themo Scientific) equipped with a 1064-nm laser at a resolution of 1 cm^{-1}. The spectrometer was placed in a dry room (dew point −60 ºC) to avoid exposing the samples to the ambient air atmosphere. The spectra were all calibrated by the polypropylene standard. To analyze the representative Raman bands, suitable spectral ranges were adopted in this study: 800–920 and 720–770 cm^{-1} for the G4 and $[TFSA]^-$ anions, respectively.

X-ray crystallography was performed on single crystals of $[Mg(G4)(DPSO_2)_2][TFSA]_2$, $[Mg(EIm)_6][TFSA]_2$, $[Mg(G4)(MIm)_2][TFSA]_2$, and $[Mg(DMSO)_6][TFSA]_2$ obtained by slow condensation of the corresponding acetonitrile solutions or grown from ionic liquid solutions. Each crystal coated with Parabar 10312 (Hampton Research) was mounted on a glass fiber and cooled to -100 ºC using a steady flow of nitrogen gas. All measurements were made on a Rigaku XtaLab Pro diffractometer using multilayer mirror mono-chromated Mo-Kα radiation (λ = 0.71073 Å). Reflection data were collected and processed using CrysAlisPro (Rigaku Oxford Diffraction). An empirical absorption correction was applied, and the data were corrected for Lorentz and polarization effects. The structures were solved by the direct methods of SHELXT 2014/4[46] and were refined using full-matrix least-squares in an anisotropic approximation for non-hydrogen atoms using SHELXL 2014/7.[47] All hydrogen atoms were placed in geometrically ideal positions and refined using an isotropic riding model. The crystallographic information file was deposited in the Cambridge Structure Database (CSD) as CCDC 1909206, 1900782, 1900781, and 1900780 for $[Mg(G4)(DPSO_2)_2][TFSA]_2$, $[Mg(EIm)_6][TFSA]_2$, $[Mg(G4)(MIm)_2][TFSA]_2$, and $[Mg(DMSO)_6][TFSA]_2$, respectively. The detailed crystallographic data are summarized in Table S1.

The density functional theory (DFT) calculations was performed by Gaussian16 Revision A.03 code,[48] using M06 hybrid functional and 6-311++G(d,p) basis set.[49] The integral equation formalism polarizable continuum model (IEFPCM) was used to model the solvation effects. The geometry optimization and HOMO-LUMO energies of the free solvent, free anion in the solvent, and anion coordinating to Mg^{2+} in solvent are performed with M06/6-311++G(d,p) level of theory and a polarizable continuum model (IEFPCM) for G3 (ε = 7.62).

A galvanostatic charge–discharge test was performed on the Mg-$MgCo_2O_4$ and Mg-$MgMn_2O_4$ cells using a three-electrode-type cell. The composite cathode was fabricated by thoroughly mixing $MgCo_2O_4$ or $MgMn_2O_4$ as the active material, acetylene black (Denka) as an electrically conductive support, and poly(1,1,2,2-tetrafluoroethylene) (PTFE) as a binder in weight ratios of 60:30:10. The PTFE paste was spread onto Pt or Al mesh current collectors and compressed at 8 MPa to improve the electrical conductivity. A three-electrode-type cell consisting of a $MgCo_2O_4$ or $MgMn_2O_4$ composite positive electrode, a magnesium ribbon negative electrode, a Ag/Ag^+ reference electrode (*vide supra*), and the electrolytes was assembled in the glovebox. A cycling test was carried out at a rate of 1/25 C based on the mass of active materials at 100 ºC with a limited capacity condition. The charging capacity was limited to half the theoretical capacity in order to suppress the undesired anodic decomposition of the electrolytes (Figure S1). The cell was initially discharged until it reached the discharge cutoff voltage of −1.0 V *vs*. the reference, which corresponds to +1.6 V *vs*. Mg/Mg^{2+}. It was then charged using an automatic charge/discharge instrument (HJ1001SD8, Hokuto Denko). The subsequent cycles were measured under the same conditions as before.

Results and Discussions

Compatibility of ionic liquids with magnesium metal: Owing to the relatively negative electrode potential of the magnesium metal, *i.e*., −2.36 V *vs*. SHE, the metal can reduce (or simply react with) various materials in contact. Indeed, diverse solvents and anions including carbonate, nitrile, tetrafluoroborate, and hexafluorophosphate readily react with the magnesium metal, resulting in surface passivation.[36,50–52] On the other hand, ethereal solutions of hexamethyldisilazide or $[TFSA]^-$

allow for highly reversible magnesium deposition/dissolution, especially with the coexistence of Cl-based compounds.[14,53–56] These observations strongly suggest the significance of a suitable choice of anions in the MRB electrolytes. To achieve IL-based electrolytes that allow for reversible magnesium deposition/dissolution, the compatibility of ILs having thermally stable amide-type anions with magnesium metal was investigated as a preliminary survey.

Figure 1 summarizes the atomic magnesium abundance on the surface of the magnesium strips soaked in four different ILs for 24 h at 25 and 100 ºC, evaluated by EDX analysis. The strips for the test were mechanically polished and subsequently treated with C_2H_5MgCl-$AlCl_3$/THF to remove any residual oxide on the surface. The surface of the reference strip was confirmed to have a 99% purity of Mg. As shown in Figure 1, the concentration of magnesium on the surface decreased upon soaking in any ILs, suggesting that some undesired reactions took place irrespective of the choice of anions even though no current was applied. The reactivity, however, seems different depending the anion structure. For $[TFSA]^-$, the concentration of magnesium on the surface was maintained at a high level of 95% even at 100 ºC, indicating remarkable cathodic and thermal stability. On the other hand, the surface was covered by reaction products for the other anions. In particular, the concentration of magnesium significantly decreased and a large amount of decomposition products was detected on the surface of $[DCA]^-$ even at 25 ºC. This strongly indicated that the nitrile group was sensitive toward magnesium metal. This observation also supports the inability of acetonitrile-based electrolytes for magnesium deposition.[51,52]

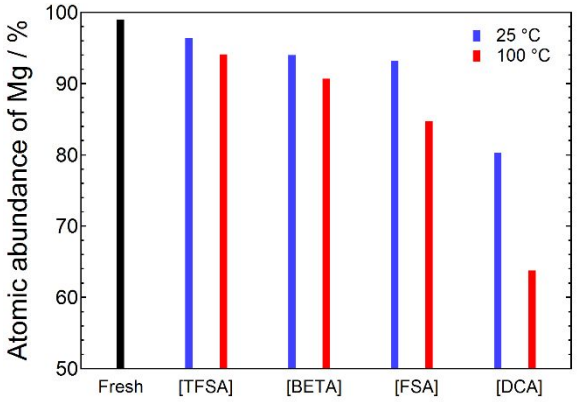

Figure 1. Surface atomic magnesium abundance of magnesium strips after soaking in each IL for 24 h at 25 and 100 ºC.

As the ILs with $[TFSA]^-$ families, which can be employed as electrolytes for lithium battery applications, operated at moderate temperatures,[57] relatively poor magnesium abundance on the strip soaked in the $[FSA]^-$ IL certainly arises from the intrinsic instability of the anion toward the magnesium metal. The XPS spectra of the soaked magnesium strips clearly illustrate the presence of reaction products mainly derived from anions (Figure S2). No or very minor contributions of fluorine, sulfur, and nitrogen-based compounds were found for $[TFSA]^-$, while the peaks assignable to MgF_2, C-F compounds, and $MgSO_4$ were discernible for $[FSA]^-$ and $[BETA]^-$. The difference observed in the relative intensity between the MgF_2 and C-F compounds for $[FSA]^-$ and $[BETA]^-$ can be explained in terms of the structure of the anions. It has been reported that sulfonylamide-type anions reductively decompose through bond cleavage at N—S···R (R = F or C_nF_{2n+1}) sites.[58–60] Thus, fluorine radical is released through the $[FSA]^-$ decomposition process and readily reacts with magnesium metal to be MgF_2 (Figure S2a), which is known as an insulator. This is why a [FSA]-based IL electrolyte is unable to be used in MRB applications.[61] The N1s spectra also demonstrate the poor stability of $[DCA]^-$ in

contact with magnesium metal, as a strong peak assignable to N-Mg compounds was clearly observed (Figure S2c).

The stability of $[TFSA]^-$ families during the magnesium deposition/dissolution process was further assessed by cyclic voltammetry (CV). As neat ILs themselves are inactive for magnesium deposition/dissolution, each IL was mixed with Grignard reagent C_2H_5MgCl/THF in a 1:1 volume ratio. The CV curves of a series of IL-Grignard reagent mixtures illustrate the anion-dependent electrochemical behavior, reflecting the stability of IL anions. The mixture with $[TFSA]^-$ showed favorable magnesium deposition/dissolution behavior, while that with $[BETA]^-$ was moderate and in good agreement with the EDX and XPS analyses. A peculiar behavior was observed for the mixture incorporating $[FSA]^-$ where the magnesium deposition/dissolution redox potential was shifted to the cathodic side by *ca*. 0.6 V. The CV measurements of this electrolyte were conducted for three times, and similar results were reproducible. Although we have no clear explanation for this shift in the magnesium redox potential, contamination of the reference electrode during measurements is one possible reason, as the reference electrolyte was indeed gradually discolored upon soaking the electrode into the [FSA]-electrolyte. The undesired side-reactions between $[FSA]^-$ and nucleophiles may induce such contamination.[62]

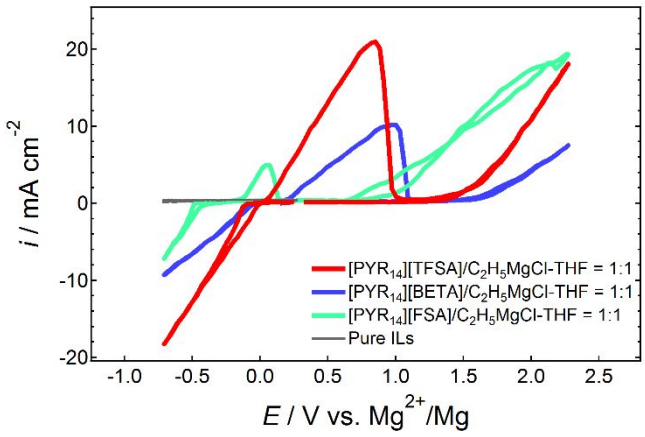

Figure 2. CV curves of binary mixtures of ILs and Grignard reagent C_2H_5MgCl-THF recorded on Pt working electrode. Scan rate, 20 mV s^{-1}; sweep range, −0.7 – +2.3 V *vs*. Mg^{2+}/Mg; temperature, 25 ºC.

The EDX analysis on the deposits obtained from the IL–Grignard reagent mixed electrolytes is also useful in evaluating which amide-type anion possesses sufficient cathodic stability during the magnesium deposition process. The deposits were obtained by potentiostatic polarization at −0.7 V *vs*. Mg^{2+}/Mg for 1 h in the different mixed electrolytes. The morphology of the deposits changed with the presence of ILs irrespective of the choice of anion structure. Granular magnesium particles, typically observed for ethereal solutions of $Mg[TFSA]_2$,[35] were homogeneously deposited on the Pt working electrode in the mixed electrolytes (Figure S3). The concentration of magnesium in the deposits, however, strongly depends on the anion structure: 88.6, 44.1, and 29.5% for $[TFSA]^-$, $[BETA]^-$, and $[FSA]^-$ containing electrolytes, respectively. As can easily be anticipated from the results of the soak tests and the XPS analysis, the cathodic decomposition of electrolytes was also involved during the magnesium deposition process for the electrolytes with $[BETA]^-$ and $[FSA]^-$. By contrast, remarkably high-purity magnesium metal can be deposited from the mixed electrolyte incorporating $[TFSA]^-$,

suggesting that the presence of $[TFSA]^-$ does not interfere with the magnesium deposition. The relatively high stability of $[TFSA]^-$ compared to those of the other amide-type anions is a likely reason.

In all, $[TFSA]^-$ was found to be particularly stable toward magnesium. Based on the preliminary survey described above, IL-based electrolytes incorporating $[TFSA]^-$ were prepared, and their electrochemical properties were studied.

Basic electrochemistry of ionic liquid-based electrolytes: Similar to observations of preceding works,[36,61] a simple electrolyte solution of $Mg[TFSA]_2$ dissolved in a typical aprotic IL $[PYR_{13}][TFSA]$ was inactive for the magnesium deposition/dissolution reaction, as evidenced by the CV curves shown in Figure 3a. This is considered to be mainly owing to the strong binding of divalent Mg^{2+} by $[TFSA]^-$, making species exist in the solution-neutral $Mg[TFSA]_2$ or aggregate $\{Mg[TFSA]_n\}^{n-2}$ ($n > 2$).[63] Such an undesired situation can be easily solved by modifying the coordination structure of the magnesium species. Modestly reversible behavior was clearly observed for the electrolytes containing G4 (Figure 3a), suggesting that the complexation of magnesium species with G4 imparts electrochemical activity.

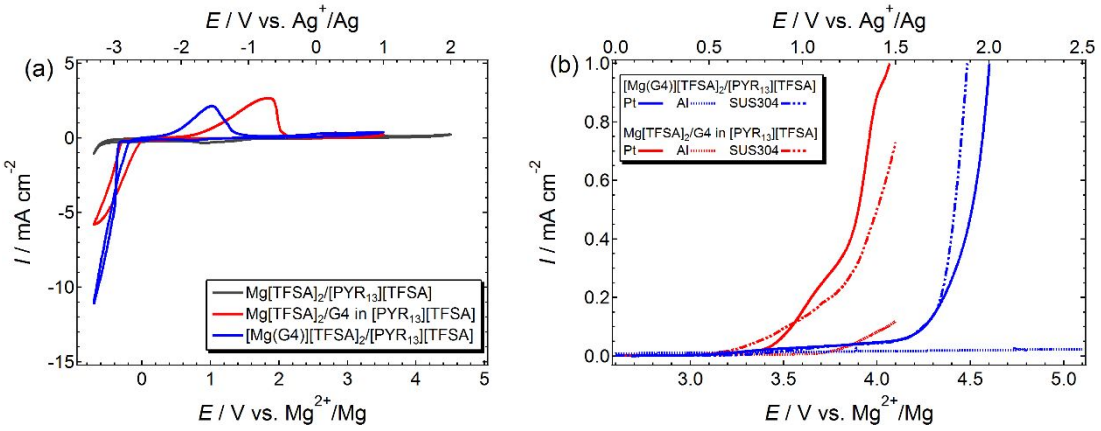

Figure 3. (a) Cyclic voltammograms (CVs) of $Mg[TFSA]_2$, $Mg[TFSA]_2$/G4 (1/5 in molar ratio), and $[Mg(G4)][TFSA]_2$ dissolved in $[PYR_{13}][TFSA]$ recorded on Pt working electrode at scan rate of 50 mV s^{-1} at

100 ºC. Concentration of $Mg[TFSA]_2$ in each solution was fixed at 0.5 mol dm^{-3}. (b) LSV curves of Pt, Al, and SUS304 current collectors measured in $Mg[TFSA]_2$/G4 and $[Mg(G4)][TFSA]_2$ dissolved in $[PYR_{13}][TFSA]$ at 100 ºC at scan rate of 1 mV s^{-1}.

It has been reported that binary mixtures of $Mg[TFSA]_2$ and G4 form an equimolar complex, $[Mg(G4)][TFSA]_2$.[38,43] In this complex structure, as almost all G4 molecules participate in Mg^{2+} coordination and are strongly polarized by the strong electric field of divalent Mg^{2+} ions, the complex possesses exceptionally high thermal and electrochemical stability compared to the electrolyte solutions of $Mg[TFSA]_2$/G4, which contain a certain amount of uncoordinated G4 molecules. The oxidative stability of IL-based electrolytes clearly reflects whether uncoordinated G4 molecules exist in the solutions. As shown in Figure 3b, an anodic current increase was observed at *ca*. 3.4 V *vs*. Mg^{2+}/Mg on Pt for the electrolyte prepared by dissolving $Mg[TFSA]_2$ in the hybrid G4 and $[PYR_{13}][TFSA]$. This anodic current was attributed to the oxidative decomposition of uncoordinated G4.[43,64] Note that, an anodic limit of the hybrid electrolyte was slightly lower on Al. This is partly due to Al corrosion, as shown in Figure S4. The oxidative stability was, however, significantly improved by controlling the molar ratio between $Mg[TFSA]_2$ and G4. The anodic limit of the IL-based electrolyte incorporating equimolar complex $[Mg(G4)][TFSA]_2$ reached 4.1 V or higher *vs*. Mg^{2+}/Mg on Pt or Al working electrodes without the loss of its electrochemical magnesium deposition/dissolution activity. The absence of relatively unstable uncoordinated G4 molecules in $[Mg(G4)][TFSA]_2$/$[PYR_{13}][TFSA]$ leads to an enhanced oxidative stability. The detailed coordination environment of Mg^{2+} in the electrolyte will be discussed later. The current density and reversibility of

magnesium deposition/dissolution for $[Mg(G4)][TFSA]_2/[PYR_{13}][TFSA]$ is particularly sensitive to the concentration of the complex (Figure S5). Owing to the electrochemical activity, the concentration is fixed hereafter at 0.5 mol dm^{-3} for further experimentation.

As described above, the coordination environment of Mg^{2+} in the electrolyte solutions has a significant impact on the electrochemical behavior. The coordination manner of glymes and $[TFSA]^-$ anions in glyme–salt mixtures can be evaluated by analyzing the corresponding vibrational modes. The Raman spectra of the $[Mg(G4)][TFSA]_2/[PYR_{13}][TFSA]$ and its ingredients recorded at ambient temperature are summarized in Figure 4. A characteristic intense band is clearly observed at 890 cm^{-1} for $[Mg(G4)][TFSA]_2$ and is readily assignable to ring-breathing mode (Figure 4).[43] This band is well-known as the fingerprint for the complex formation of [M(glyme)] species irrespective of the glyme length, anion structure, and coordination center.[64,65] Uncoordinated glymes have a broad band in the range 850–800 cm^{-1} owing to a combination of various CH_2 rocking and CO stretching modes for many different conformers.[66] The spectrum for the binary mixture of $Mg[TFSA]_2$ and G4 showed features of $[Mg(G4)][TFSA]_2$ and uncoordinated G4, indicating both species presented in the solution. In stark contrast, no feature of uncoordinated G4 was discernible at 850 cm^{-1} for $[Mg(G4)][TFSA]_2/[PYR_{13}][TFSA]$, while the band assignable to the glyme–Mg complex was still observed even in the IL solution. Although the bands owing to inter/intramolecular vibrational modes of $[PYR_{13}]^+$ unfortunately overlapped, such a spectral shape strongly suggested that the presence of $[PYR_{13}][TFSA]$ would not disrupt the structure of $[Mg(G4)]^{2+}$ ions.

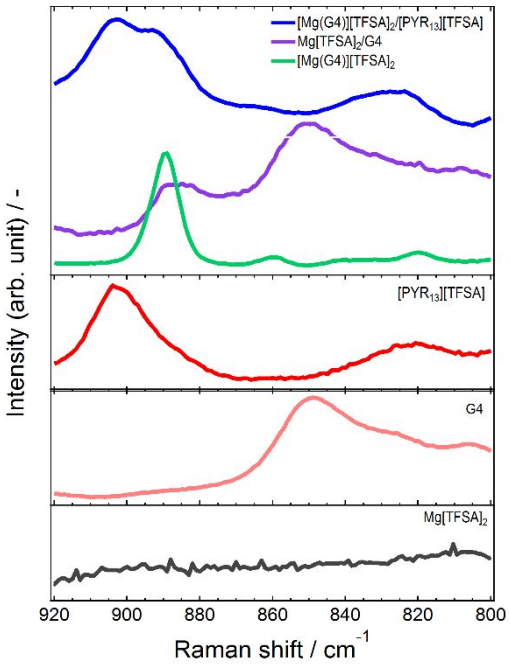

Figure 4. Raman spectra of complex electrolytes and ingredients recorded at ambient temperature. Spectral range was adopted for coordination state of G4.

Galvanostatic charge–discharge cycling of the high-voltage positive electrode material $MgCo_2O_4$ was performed by using a three-electrode cell with the IL electrolyte in order to assess the high oxidative stability of this electrolyte. To suppress the undesired electrolyte decomposition during charging, the charging capacity was limited to 130 mAh g^{-1} (half the theoretical capacity of $MgCo_2O_4$). The capacity-limited charge–discharge profiles demonstrated a relatively stable cycling of [Mg || $MgCo_2O_4$] cells with the [Mg(G4)][TFSA]$_2$/[PYR_{13}][TFSA] electrolyte irrespective of the choice of current collectors, while the cells could not be charged well by using the hybrid Mg[TFSA]$_2$/G4-[PYR_{13}][TFSA] electrolyte owing to its relatively poor oxidative stability (Figure 5). An EDX analysis on the surface of the cycled Mg metal negative electrodes clearly demonstrated the suppression of the undesired anodic dissolution of Co by using the IL-based electrolyte, as no trace of Co was detected

(Figure 6a). In stark contrast, a certain amount of Co was dissolved and accumulated on the cycled Mg electrode for the hybrid Mg[TFSA]$_2$/G4-[PYR$_{13}$][TFSA] electrolyte. The difference in these cycling behaviors arises from the intrinsic coordinating ability and oxidative stability of the electrolyte solvents, and an IL-based electrolyte incorporating appropriate supporting salts is likely suitable for HV-MRB applications. It is noteworthy that the deliverable capacity decreased upon cycling even with the [Mg(G4)][TFSA]$_2$/[PYR$_{13}$][TFSA] electrolyte (Figure 5a). This possibly comes from undesired decomposition of the electrolytes at $MgCo_2O_4$, due to the catalytic activity of Co-based oxide materials.[67]

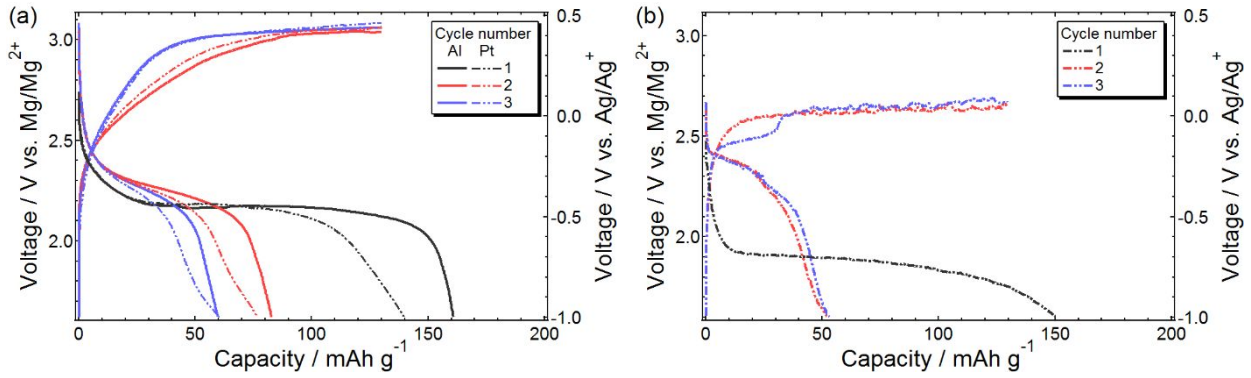

Figure 5. Galvanostatic charge–discharge curves of [Mg | electrolyte | $MgCo_2O_4$] cells measured at 100 ºC. (a) 0.5 mol dm^{-3} [Mg(G4)][TFSA]$_2$/[PYR$_{13}$][TFSA] and (b) 0.5 mol dm^{-3} hybrid Mg[TFSA]$_2$/G4-[PYR$_{13}$][TFSA].

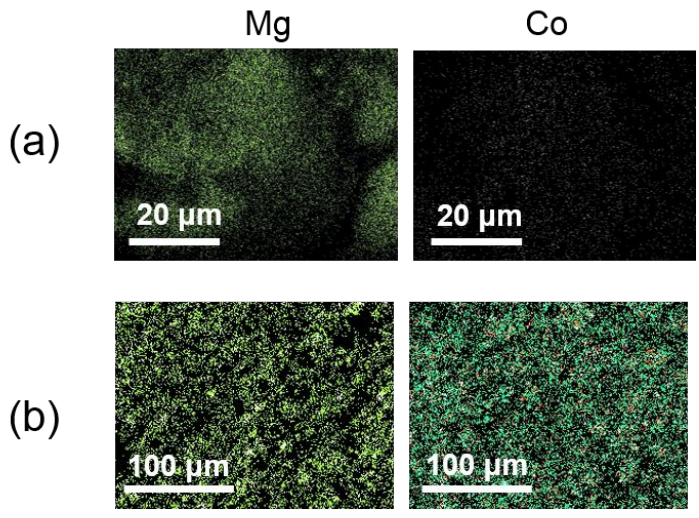

Figure 6. SEM-EDX analysis of magnesium electrodes cycled with $MgCo_2O_4$ composite electrodes in (a) 0.5 mol dm^{-3} $[Mg(G4)][TFSA]_2/[PYR_{13}][[TFSA]$ and (b) 0.5 mol dm^{-3} hybrid $Mg[TFSA]_2$/G4-$[PYR_{13}][TFSA]$.

Modifications to structure of $Mg[TFSA]_2$-based supporting salt: The oxidative stability of $[Mg(G4)][TFSA]_2/[PYR_{13}][TFSA]$ reaches a level that is high enough for HV-MRB applications. The poor Coulombic efficiency for the magnesium deposition/dissolution reaction, however, should be improved for the realization of practical batteries. The deposits obtained by potentiostatic polarization from this electrolyte contain considerably small amount of magnesium (*ca*. 10% in atomic concentration) but a significantly large portion of fluorine-, oxygen-, sulfur-, and nitrogen-based compounds, strongly implying that magnesium deposition involves the reductive decomposition of $[TFSA]^-$. The atomic concentration of magnesium in the deposits obtained from the hybrid electrolyte was *ca*. 30%, slightly higher than that from $[Mg(G4)][TFSA]_2/[PYR_{13}][TFSA]$. Nevertheless, the high cathodic stability of $[TFSA]^-$ during the magnesium deposition process was certainly confirmed in the preliminary survey (*vide supra*). The cathodic instability of $[TFSA]^-$, particularly in the magnesium battery electrolytes, was reported previously. Persson et al. simulated the reduction mechanism of $[TFSA]^-$ at the interface between the electrolyte and Mg electrode, and found that $[TFSA]^-$ bound to the Mg cation center is easily reduced.[68] Matsui et al. experimentally observed the formation of passivation layer through the reductive decomposition of $[TFSA]^-$ during a cathodic scan by using an in-situ FT-IR technique for ethereal solutions of $Mg[TFSA]_2$.[44] They further confirmed the interfacial behavior of magnesium alloy electrodes in the acetonitrile and glyme solutions containing $Mg[TFSA]_2$ to be predominated by the coordination state of $[TFSA]^-$.[69] We also calculated the lowest-unoccupied

molecular orbital (LUMO) energy levels of $[TFSA]^-$ in two different coordination states, coordinated to Mg^{2+} or not (free), by density functional theory (DFT) calculation using a polarizable continuum model for G3 (ε = 7.62). The LUMO energy level of $[TFSA]^-$ was indeed lowered upon coordination with Mg^{2+}, from −0.37 to −1.86 eV (which corresponds to *ca*. −1.7 to −0.2 V *vs*. Mg^{2+}/Mg). On the basis of these preceding works and our results, it can be considered that $[TFSA]^-$ that is in contact with Mg^{2+} is highly polarized, and such polarization makes $[TFSA]^-$ unstable toward reduction.

The coordination state of $[TFSA]^-$ can be qualified by analyzing certain vibrational modes. The expansion-contraction mode of $[TFSA]^-$ is particularly suitable to characterize the $[TFSA]^-$ coordination because the corresponding band position shifts depending on the coordination state of $[TFSA]^-$: a solvent-separated ion pair (SSIP) or free, contact ion pair (CIP), and aggregate (AGG) are characterized in general at 739–742, 743–747, and >747 cm^{-1}, respectively.[70,71] The Raman spectra of $[Mg(G4)][TFSA]_2$/$[PYR_{13}][TFSA]$ are summarized in Figure S6a. The bands for $Mg[TFSA]_2$ and $[PYR_{13}][TFSA]$, which are prone to form AGG and SSIP were observed at 750 and 740 cm^{-1}, respectively. As the $[TFSA]^-$ directly coordinates to Mg^{2+} ions to form CIP-type solvates in the crystalline $[Mg(G4)][TFSA]_2$,[37,56] the corresponding Raman band should be located at approximately 743–747 cm^{-1} and indeed was found at 744 cm^{-1}. The deconvolution and fitting of the broad band observed for $[Mg(G4)][TFSA]_2$/$[PYR_{13}][TFSA]$ revealed the presence of $[TFSA]^-$ in different coordination states. The band can be deconvoluted into two bands at 741 and 744 cm^{-1}, readily assignable to SSIP and CIP, respectively (Figure S6b). The presence of relatively great amount of the CIP-[TFSA] is one possible reason for the poor magnesium deposition/dissolution efficiency of $[Mg(G4)][TFSA]_2$/$[PYR_{13}][TFSA]$.

One of the most straightforward approaches to make $[TFSA]^-$ free is simply adding chloride-based compounds. Owing to the remarkably stronger Lewis basicity of Cl^- over that of $[TFSA]^-$, Cl^- preferentially coordinates to Mg^{2+}. Indeed, the structures of magnesium complexes formed in $Mg[TFSA]_2/MgCl_2$/glyme solutions were recently revealed as multinuclear Mg-Cl complexes paired with $[TFSA]^-$ in the SSIP state,[72] while CIP-[TFSA] exists slightly in typical Cl-free ethereal solutions even at extremely low $Mg[TFSA]_2$ concentrations.[69] Cl-based additives effectively enhance the efficiency for $[Mg(G4)][TFSA]_2/[PYR_{13}][TFSA]$ almost irrespective of the choice of Cl source, as shown in Figure S7a. These compounds, however, simultaneously cause poor oxidative stability and severe corrosion toward various battery substrates (Figure S7b). Thus, it is extremely difficult to apply such electrolytes to HV-MRBs.

As there is competition for the mutual interactions of cations with solvents (ligands) and anions in typical electrolyte solutions, the anion coordination state can be modified by controlling the coordination ability of the ligands. Owing to the reasonable coordination ability and electrochemical stability,[73] a series of dialkyl sulfone was selected as ligands and was added to $[Mg(G4)][TFSA]_2$ in a 1:2 molar ratio. Single crystals of $[Mg(G4)(DPSO_2)_2][TFSA]_2$ were successfully isolated from the IL solution. X-ray crystallography clearly revealed that the coordination state of $[TFSA]^-$ is modified by using dialkyl sulfone (Figure 7). In the $[Mg(G4)(DPSO_2)_2][TFSA]_2$ crystal, Mg^{2+} is surrounded by a single G4 molecule in a characteristic coordination manner, as observed in $[Mg(G4)][TFSA]_2$. Instead of $[TFSA]^-$, two $DPSO_2$ molecules further coordinate to Mg^{2+} perpendicularly, thereby resulting in a sevenfold coordination sphere. No $[TFSA]^-$ participates in Mg^{2+} coordination in the $[Mg(G4)(DPSO_2)_2][TFSA]_2$ crystal. The bond distances between Mg^{2+} and oxygen atoms of $[TFSA]^-$

in $[Mg(G4)][TFSA]_2$ and $DPSO_2$ in $[Mg(G4)(DPSO_2)_2][TFSA]_2$ are 2.044–2.058 and 2.039–2.057 Å, respectively, suggesting comparable interactions of $[Mg(G4)]^{2+}$ with $[TFSA]^-$ and $DPSO_2$.

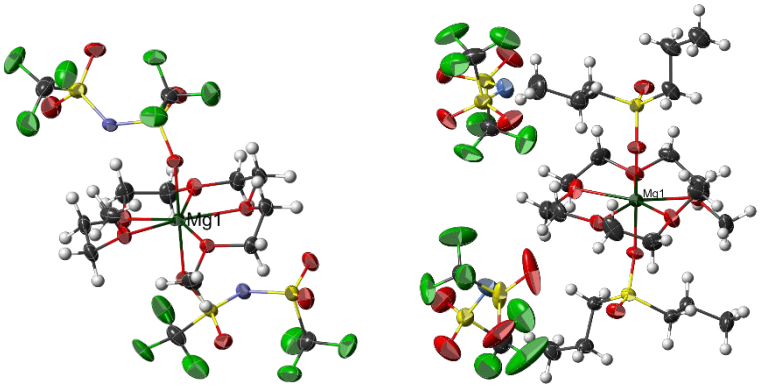

Figure 7. Thermal ellipsoid models of (left) $[Mg(G4)][TFSA]_2$ and (right) $[Mg(G4)(DPSO_2)_2][TFSA]_2$. Ellipsoids of non-hydrogen atoms are drawn at 50% probability level, while isotropic hydrogen atoms are represented by arbitrary spheres. Structure of $[Mg(G4)][TFSA]_2$ was reproduced from CCDC 1420478 (Cambridge Structure Database). Dark green, Mg; gray, C; white, H; red, O; light green, F; light blue, N; yellow, S.

The coordination state of $[TFSA]^-$ in the complexes incorporating G4 and various dialkyl sulfones was further assessed by Raman spectroscopy. Figure 8 displays the Raman spectra of $[Mg(G4)(sulfone)_2][TFSA]_2$ recorded at ambient temperature. The spectra of $[Mg(G4)][TFSA]_2$ and G4 are also included as references. In each complex, G4 is found to still coordinate with Mg^{2+} in a similar manner to that in the $[Mg(G4)][TFSA]_2$ crystal, as evident from observation of the ring-breathing mode with no peak shifts. On the other hand, the expansion-contraction mode of $[TFSA]^-$ obviously shifts to the low-frequency side (from 744 to 741 cm^{-1}) upon the addition of any dialkyl sulfone. The resulting peak position is readily assignable to free or SSIP $[TFSA]^-$. These results strongly suggest the formation of a $[Mg(G4)(sulfone)_2]^{2+}$ cation paired with isolated $[TFSA]^-$ upon

the complexation of $[Mg(G4)][TFSA]_2$ with sulfone. Such a unique coordination structure of $[Mg(G4)(sulfone)_2][TFSA]_2$ is maintained even after the complexes dissolve in the IL (Figure S8). The peak assignable to coordinated $[TFSA]^-$ did indeed disappear after sulfone was added to $[Mg(G4)][TFSA]_2/[PYR_{13}][TFSA]$.

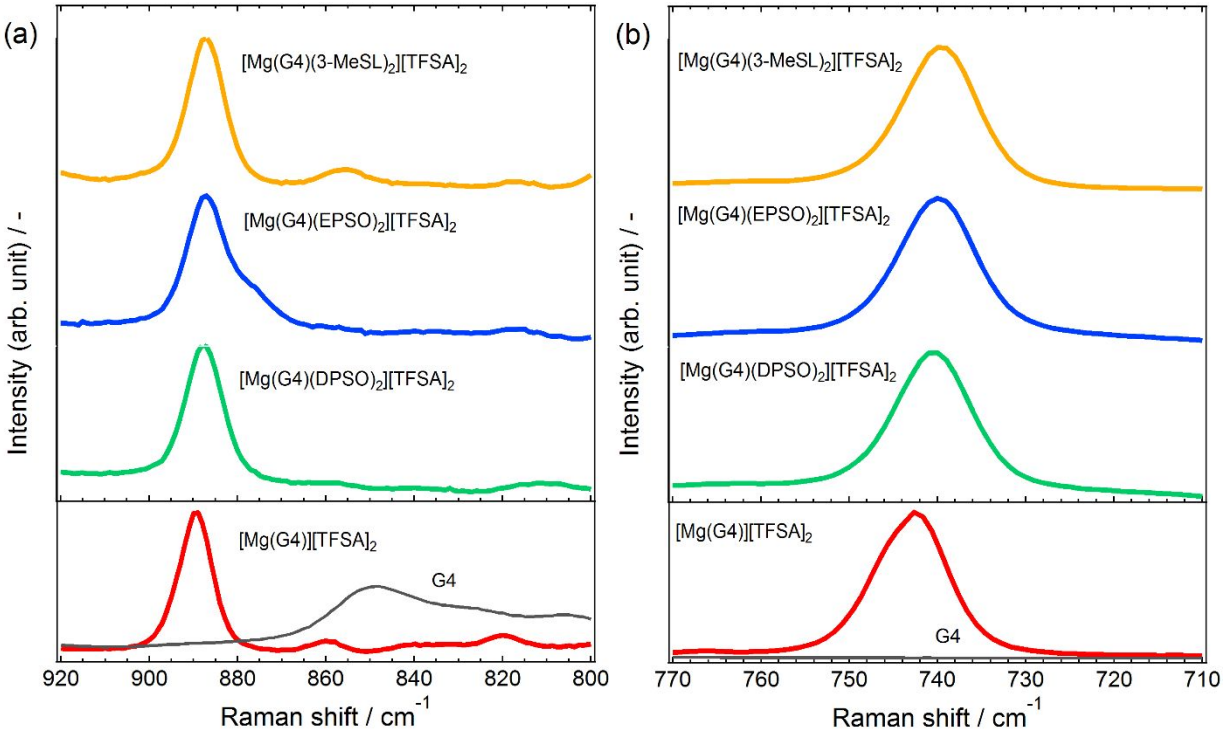

Figure 8. Raman spectra of $[Mg(G4)(dialkyl\ sulfone)_2][TFSA]_2$ recorded at ambient temperature. Specific spectral range was adopted for coordination state of (a) G4 and (b) [TFSA].

The electrochemical activity of the $Mg[TFSA]_2$-based complexes having isolated (SSIP) $[TFSA]^-$ was examined by CV. As shown in Figure 9a, the molten $[Mg(G4)][TFSA]_2$ is barely active electrochemically, mainly owing to strong Mg-[TFSA] interactions and thus the poor reductive stability of $[TFSA]^-$ during a cathodic scan. The electrochemical activity was significantly enhanced by adding two molar equivalent sulfones to the equimolar mixture of $Mg[TFSA]_2$ and G4. Somewhat reversible cathodic and anodic currents were clearly observed for $[Mg(G4)(EPSO_2)_2][TFSA]_2$ and

$[Mg(G4)(EMSO_2)_2][TFSA]_2$. The electrolytes of the modified $Mg[TFSA]_2$ complexes dissolved in $[PYR_{13}][TFSA]$ showed further favorable electrochemical properties. The cycling reversibility was significantly improved by using the modified complex electrolytes (Figure 9b). The atomic concentration of magnesium in the deposits obtained from the electrolytes improved significantly from 10% for $[Mg(G4)][TFSA]_2$/$[PYR_{13}][TFSA]$ to 53% for $[Mg(G4)(EPSO_2)_2][TFSA]_2$/$[PYR_{13}][TFSA]$, clearly indicating the suppression of the reductive decomposition of $[TFSA]^-$ during magnesium deposition by controlling the coordination state of $[TFSA]^-$. The anodic limits of the IL electrolytes incorporating modified complexes still maintained high levels above +3.5 V *vs*. Mg^{2+}/Mg even at 100 ºC. Therefore, making a coordination state of $[TFSA]^-$ SSIP in electrolytes is particularly effective in improving the electrochemical activity without losing the high thermal and anodic stability. Note that the electrolyte with 3-MeSL showed negligible cathodic and anodic responses. We have no clear explanation of this observation, but the cyclic structure may affect the Mg-ligand interactions, consequently leading to poor electrochemical activity.

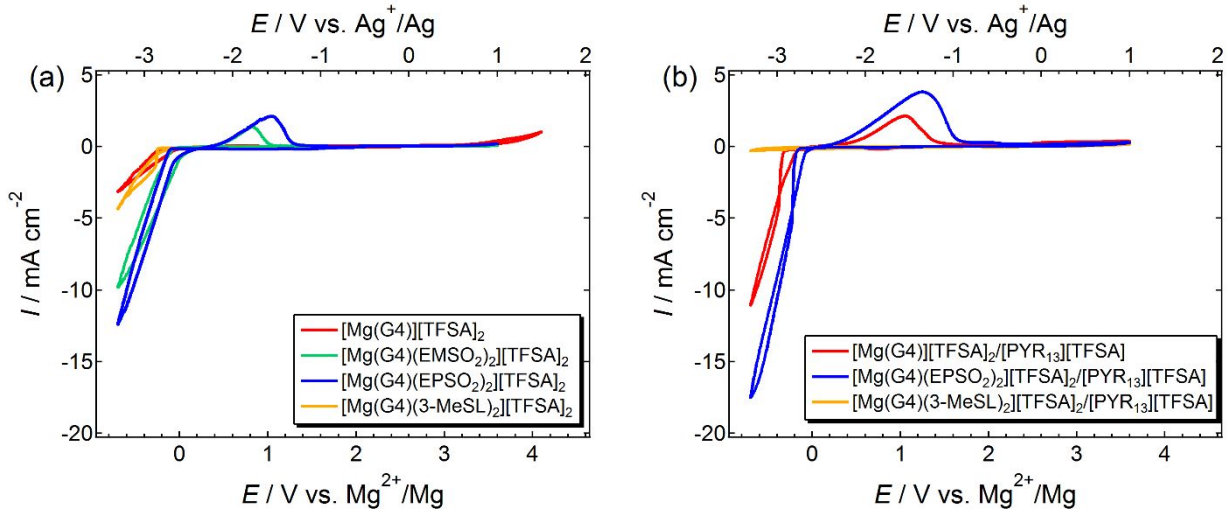

Figure 9. CV curves of (a) $Mg[TFSA]_2$-based complexes and (b) those dissolved in $[PYR_{13}][TFSA]$, recorded on Pt working electrode at scan rate of 50 mV s^{-1} at elevated temperature (100 or 150 °C).

The galvanostatic charge–discharge characteristics of $MgMn_2O_4$ with the modified electrolytes were studied by using three electrode cells. Figure 10 illustrates the charge–discharge curves of [Mg | electrolyte | $MgMn_2O_4$] cells with IL electrolytes incorporating $[Mg(G4)][TFSA]_2$ or $[Mg(G4)(EPSO_2)_2][TFSA]_2$ as supporting salts. As expected, the cycling behavior of the [Mg || $MgMn_2O_4$] cells was improved after modifying the structure of the supporting salts. The electrolyte with the modified supporting salt delivered an initial discharge capacity of 252 mAh g^{-1}, while the nonmodified version had a capacity of 171 mAh g^{-1}. For subsequent cycles, relatively stable cycling behavior was observed for the cell with the modified supporting salt. The discharge capacities of the fourth cycle were 116 and 95 mAh g^{-1} for the modified and nonmodified electrolytes, respectively. The capacity fading again observed is likely due to decomposition of the electrolytes caused by transition-metal oxides.[67] In addition to the capacities, the polarization for charging and discharging was also improved by using the modified supporting salt. Although the cell voltage was controlled by the reference electrode, the activity of magnesium deposition/dissolution affected the reaction kinetics and consequently the cell voltage.

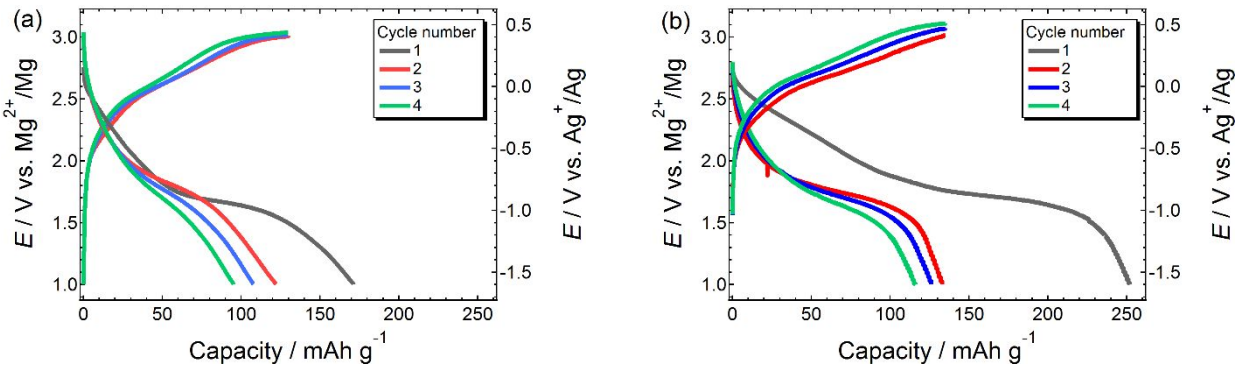

Figure 10. Galvanostatic charge–discharge profiles of $MgMn_2O_4$ measured by using three-electrode cells operated at 100 ºC at 1/25 C rate (which corresponds to 10.4 mA g^{-1} based on mass of $MgMn_2O_4$) with (a) $[Mg(G4)][TFSA]_2/[PYR_{13}][TFSA]$ and (b) $[Mg(G4)(EPSO_2)_2][TFSA]_2/[PYR_{13}][TFSA]$ (c_{Mg} = 0.5 mol dm^{-3}).

As demonstrated above, the electrolytes with isolated (SSIP-type) $[TFSA]^-$ anions exhibited better electrochemical performance than those with associated (CIP-type) anions. There are some reports on $Mg[TFSA]_2$ complexes consisting of fully solvated Mg^{2+} complex cations and SSIP $[TFSA]^-$ anions, *e.g.*, $[Mg(H_2O)_6][TFSA]_2{\cdot}2H_2O$,[74] $[Mg_2(\mu\text{-}Cl)_2(DME)_4][TFSA]_2$,[72] $[Mg(CH_3CN)_6][TFSA]_2$,[75] and $[Mg(C_2H_5OH)_6][TFSA]_2$.[76] $[Mg_2(\mu\text{-}Cl)_2(DME)_4][TFSA]_2$ is well known as an active ingredient, while electrolytes containing H_2O, CH_3CN, or C_2H_5OH are inactive for Mg^{2+}/Mg redox owing to a severe passivation of the surface of the magnesium metal induced by reductive decomposition or undesired side reactions of magnesium metal with these ligand molecules. As various metal complexes with RIm ligands and $[TFSA]^-$ or different anions are electrochemically active for the corresponding metal deposition/dissolution,[77–80] the $Mg[TFSA]_2$ complexes incorporating RIm ligands can also be regarded as potential active species. DMSO molecules also strongly coordinate with metal salts, thereby resulting in SSIP-type complexes with a variety of anions.[80–82] The formation of SSIP-type complexes was confirmed for various homoleptic and heteroleptic complexes such as $[Mg(EIm)_6][TFSA]_2$, $[Mg(G4)(MIm)_2][TFSA]_2$, and $[Mg(DMSO)_6][TFSA]_2$ in this study (Figure S9).

In contrast to various main and transition metal complexes, the $Mg[TFSA]_2$-based SSIP-type complexes with RIm and DMSO ligands were all found to be electrochemically inactive (Figure S10).

This is possibly owing to the strong solvation of Mg^{2+} by RIm and DMSO in these complexes. In typical electrolyte solutions, the deposition of metals in general involves the desolvation process of ligands from the solvated metal ions at the interfaces of electrolytes and electrodes. Although ligands (solvents) with strong coordination ability facilitate salt dissociation and can contribute to enhancement in ion transport, such strong solvation simultaneously inhibits favorable desolvation at electrode | electrolyte interfaces and possibly leads to the cathodic decomposition of the electrolytes instead of metal deposition. The Gutmann's donor numbers (*DN*s) of MIm (47) and DMSO (29.8) are indeed substantially larger than those of glymes (19) and sulfone (14.8 for sulfolane),[83,84] suggesting that the electrochemical activity for magnesium deposition/dissolution is predominated by the solvation power of the ligands. It should be noted that the mapping based on the dielectric constants (ε_r), which are also well recognized as useful indicators for the solvation ability (polarity) of solvents, is rather scattered (Figure S11). The mapping based on these different solvent parameters strongly suggests that magnesium deposition/dissolution in $Mg[TFSA]_2$-based electrolytes is predominated by the solvation or coordination environment of Mg^{2+} instead of the dielectric effect.

Conclusion

A design concept of $Mg[TFSA]_2$-based electrolyte materials applicable to HV-MRBs was proposed. Through a comprehensive survey for the compatibility of ILs having amide-type anions with magnesium metal, $[TFSA]^-$ was found to be rather stable toward magnesium metal even at elevated temperatures. A simple electrolyte of $Mg[TFSA]_2$ dissolved in a typical IL, however, did not support electrochemical magnesium deposition/dissolution owing to the strong association of Mg^{2+}

with $[TFSA]^-$. Modification of the coordination structure of $Mg[TFSA]_2$ with appropriate ligands can solve this situation, and the appropriate salt-ligand combination with well-controlled liquid states of $[Mg(G4)][TFSA]_2/[PYR_{13}][TFSA]$ provided moderate electrochemical activity for magnesium deposition/dissolution with excellent anodic stability up to +4.1 V *vs*. Mg^{2+}/Mg, even at 100 ºC.

This outstanding anodic and thermal stability of the electrolyte allows for the cycling of HV MRBs. Despite the remarkably high anodic stability of $[Mg(G4)][TFSA]_2/[PYR_{13}][TFSA]$, the magnesium deposition/dissolution efficiency in this electrolyte is modest. DFT calculations combined with vibrational and electrochemical analyses of the electrolytes and deposits revealed the cause of the relatively poor reversibility of magnesium deposition/dissolution in $[Mg(G4)][TFSA]_2$-based electrolytes as a severe reductive decomposition of the coordinated $[TFSA]^-$ during a cathodic scan. The DFT calculation also suggested a higher cathodic stability of free $[TFSA]^-$.

The coordinated $[TFSA]^-$ anions in $[Mg(G4)][TFSA]_2$ were successfully isolated from the coordination sphere of Mg^{2+} by adding certain coordination agents with strong donating ability. This approach worked well and improved the electrochemical activity by employing dialkylsulfone as an agent for coordination exchange with $[TFSA]^-$. This improvement in the electrochemical activity enhanced the cycling ability and delivered capacity of $[MgMn_2O_4 \,||\, Mg]$ cells. In stark contrast, DMSO and alkylimidazole made the electrolytes totally inactive electrochemically, while these two compounds were also effective in isolating the coordinated $[TFSA]^-$ from $[Mg(G4)][TFSA]_2$. Mapping based on both *DN*s and ε_r strongly suggested that magnesium deposition/dissolution in $Mg[TFSA]_2$-based electrolytes is dominated by the solvation or coordination environment of Mg^{2+} instead of the dielectric effect. Although the performance of the proposed electrolyte was still

insufficient for the practical realization of HV MRBs, the rational design of electrolytes based on the solvation structures attracts growing interests especially for beyond lithium-ion battery technologies as the solvation structures controls the stability and transport properties, both critical parameters determining the battery performance.[85] The significance of the coordination and dissociation states of the supporting salts in electrolyte solutions found in this study will provide significant insight for the rational design of magnesium redox active electrolyte materials with reasonable thermal and electrochemical stabilities.

Acknowledgements

This work was partly supported by the JSPS KAKENHI (Grant No. 18K14310 to T.M.) from the Japan Society for the Promotion of Science (JSPS), and the Advanced Low Carbon Technology-Specially Promoted Research for Innovative Next Generation Batteries Program (ALCA-SPRING) of the Japan Science and Technology Agency (JST). The authors are also grateful for the kind support provided by the NIMS Battery Research Platform on Raman spectroscopy measurements.

References

1. P. Saha, M. K. Datta, O. I. Velikokhatnyi, A. Manivannan, D. Alman, P. N. Kumta, *Prog. Mater. Sci*., 2014, **66**, 1–86.

2. C. B. Bucur, T. Gregory, A. G. Oliver, J. Muldoon, *J. Phys. Chem. Lett*., 2015, **6**, 3578–3591.

3. J. Song, E. Sahadeo, M. Noked, S. B. Lee, *J. Phys. Chem. Lett*., 2016, **7**, 1736–1749.

4. R. Zhang, C. Ling, *MRS Energy Sustain*., 2016, **3**, 1–16.

5. Z. Ma, D. R. MacFarlane, M. Kar, *Batteries & Supercaps*, 2019, **2**, 115–127.

6. Z. Z.-Karger, M. Fichtner, *Front. Chem*., 2019, **6**, 656.

7. L. Kong, C. Yan, J.-Q. Huang, M.-Q. Zhao, M.-M. Titirici, R. Xiang, Q. Zhang, *Energy Environ. Mater*., 2018, **1**, 100–112.

8. M. Matsui, *J. Power Sources*, 2011, **196**, 7048–7055.

9. D. Aurbach, Z. Lu, A. Schechter, Y. Gofer, H. Gizbar, R. Turgeman, Y. Cohen, M. Moshkovich, E. Levi, *Nature*, 2000, **407**, 724–727.

10. D. Aurbach, H. Gizbar, A. Schechter, O. Chusid, H. E. Gottlieb, Y. Gofer, I. Boldberg, *J. Electrochem. Soc*., 2002, **149**, A115–A121.

11. H. D. Yoo, I. Shterenberg, Y. Gofer, G. Gershinsky, N. Pour, D. Aurbach, *Energy Environ. Sci*., 2013, **86**, 2265–2279.

12. B. P. Vinayan, Z.-Z. Karger, T. Diemant, V. S. K. Chakravadhanula, N. I. Schwarzburger, M. A. Cambaz, R. J. Behm, C. Kubel, M. Fichtner, *Nanoscale*, 2016, **8**, 3296–3306.

13. Z. Z.-Karger, M. E. G. Bardaji, O. Fuhr, M. Fichtner, *J. Mater. Chem. A*, 2017, **5**, 10815–10820.

14. H. S. Kim, T. S. Arthur, G. D. Allred, J. Zajicek, J. G. Newman, A. E. Rodnyansky, A. G. Oliver, W. C. Boggess, J. Muldoon, *Nat. Commun*., **2011**, 2:427, DOI: 10.1038/ncomms1435.

15. Z. Z.-Karger, X. Zhao, D. Wang, T. Diemant, R. J. Behm, M. Fichtner, *Adv. Energy Mater*., 2014, 1401155.

16. Z. Z.-Karger, R. Liu, W. Dai, Z. Li, T. Diemant, B. P. Vinayan, C. B. Minella, X. Yu, A. Manthiram, R. J. Behm, M. Ruben, M. Fichtner, *ACS Energy Lett*., 2018, **3**, 2005–2013.

17. X. Zhou, J. Tian, J. Hu, C. Li, *Adv. Mater*., 2018, **30**, 1704166.

18. G. Bieker, D. Diddens, M. Kolek, O. Borodin, M. Winter, P. Bieker, K. Jalkanen, *J. Phys. Chem. C*, 2018, **122**, 21770–21783.

19. C. Kim, P. J. Phillips, B. Key, T. Yi, D. Nordlund, Y.-S. Yu, R. D. Bayliss, S.-D. Han, M. He, Z. Zhang, A. K. Burrell, R. F. Klie, J. Cabana, *Adv. Mater.*, 2015, **27**, 3377–3384.

20. J.-S. Kim, W.-S. Chang, R.-H. Kim, D.-Y. Kim, D.-W. Han, K.-H. Lee, S.-S. Lee, S.-G. Doo, *J. Power Sources*, 2015, **273**, 210–215.

21. S. Okamoto, T. Ichitsubo, T. Kawaguchi, Y. Kumagai, F. Oba, S. Yagi, K. Shimokawa, N. Goto, T. Doi, E. Matsubara, *Adv. Sci*., 2015, **2**, 1500072.

22. Y. Kotani, R. Ise, K. Ishii, T. Mandai, Y. Oaki, S. Yagi, H. Imai, *J. Alloys Compd*., 2018, 739, 793–798.

23. V. Duffort, X. Sun, L. F. Nazar, *Chem. Commun*., 2016, **52**, 12458–12461.

24. F. Xiong, Y. Fan, S. Tan, L Zhou, Y. Xu, C. Pei, Q. An, L. Mai, *Nano Energy*, 2018, **47**, 210–216.

25. M. Wu, Y. Zhang, T. Li, Z. Chen, S.-A. Cao, F. Zu, *Nanoscale*, 2018, **10**, 12526–12534.

26. Z. Wang, S. Rafai, C. Qiao, J. Jia, Y. Zhu, X. Ma, C. Cao, *ACS Appl. Mater. Interfaces*, 2019, **11**, 7046–7054.

27. O. Tutusaus, R. Mohtadi, T. S. Arthur, F. Mizuno, E. G. Nelson, Y. V. Sevryugina, *Angew. Chem. Int. Ed*., 2015, **54**, 7900–7904.

28. S. G. McArthur, L. Geng, J. Guo, V. Lavallo, *Inrog. Chem. Front*., 2015, **2**, 1101–1104.

29. N. T. Hahn, T. J. Seguin, K.-C. Lau, C. Liao, B. J. Ingram, K. A. Persson, K. R. Zavadil, *J. Am.*

Chem. Soc., 2018, **140**, 11076–11084.

30. R. Jay, A. W. Tomich, J. Zhang, Y. Zhao, A. D. Gorostiza, V. Lavallo, J. Guo, *ACS Appl. Mater. Interfaces*, *ASAP*, doi: 10.1021/acsami.9b00037.

31. J. Luo, Y Bi, L. Zhang, X. Zhang, T. L. Liu, *Angew. Chem. Int. Ed*., 2019, **58**, 1–6.

32. J. T. Herb, C. A. NistLund, C. B. Arnold, *ACS Energy Lett*., 2016, **1**, 1227–1232.

33. E. N. Keyzer, J. Lee, Z. Liu, A. D. Bond, D. S. Wright, C. P. Grey, *J. Mater. Chem. A*, 2019, **7**, 2677–2685.

34. M. Liu, Z. Rong, R. Malik, P. Canepa, A. Jain, G. Ceder, K. A. Persson, *Energy Environ. Sci*., 2015, **8**, 964–974.

35. S.-Y. Ha, Y.-W. Lee, S. W. Woo, B. Koo, J.-S. Kim, J. Cho, K. T. Lee, N.-S. Choi, *ACS Appl. Mater. Interfaces*, 2014, **6**, 4063–4073.

36. G. Vardar, A. E. S. Sleightholme, J. Naruse, H. Hiramatsu, D. J. Siegel, C. W. Monroe, *ACS Appl. Mater. Interfaces*, 2014, **6**, 18033–18039.

37. A. Kitada, Y. Kang, Y. Uchimoto, K. Murase, *J. Electrochem. Soc.*, 2014, **161**, D102–D106.

38. A. Kitada, Y. Kang, K. Matsumoto, K. Fukami, R. Hagiwara, K. Murase, *J. Electrochem. Soc.*, 2015, **162**, D389–D396.

39. Z. Ma, M. Forsyth, D. R. MacFarlane, M. Kar, *Green Energy Environ*., 2018, doi: 10.1016/j.gee.2018.10.003.

40. M. Hayyan, F. S. Mjalli, M. A. Hashim, I. M AlNashef, T. X. Mei, *J. Ind. Eng. Chem*., 2013, **19**, 106–112.

41. S. P. Ong, O. Andreussi, Y. Wu, N. Marzari, G. Ceder et al., *Chem. Mater*., 2011, **23**, 2979–2986.

42. S. Yagi, A Tanaka, Y. Ichikawa, T. Ichitsubo, E. Matsubara, *Res. Chem. Intermed*., 2014, **40**, 3–9.

43. S. Terada, T. Mandai, S. Suzuki, S. Tsuzuki, K. Watanabe, Y. Kamei, K. Ueno, K. Dokko, M. Watanabe, *J. Phys. Chem. C*, 2016, **120**, 1353–1365.

44. H. Kuwata, M. Matsui, N. Imanishia, *J. Electrochem. Soc.*, 2017, **164**, A3229–A3236.

45. T. Mandai, Y. Akita, S. Yagi, M. Egashira, H. Munakata, K. Kanamura, *J. Mater. Chem. A*, 2017, **5**, 3152–3156.

46. G. M. Sheldrick, SHELXT 2014/4, *Acta Cryst*., 2014, **A70**, C1437.

47. G. M. Sheldrick, SHELXL 2014/7, *Acta Cryst*., 2008, **A64**, 112–122.

48. M. J. Frisch, G. W. Trucks, H. B. Schlegel, G. E. Scuseria, M. A. Robb, J. R. Cheeseman, G. Scalmani, V. Barone, G. A. Petersson, H. Nakatsuji, et al., Gaussian Inc, Wallingford, CT, 2016.

49. Y. Zhao, D. G. Truhlar, *Theor. Chem. Acc*., 2008, **120**, 215–241.

50. E. N. Keyzer, H. F. J. Glass, Z. Liu, P. M. Bayley, S. E. Dutton, C. P. Grey, D. S. Wright, *J. Am. Chem. Soc*., 2016, **138**, 8682–8685.

51. Z. Lu, A. Schechter, M. Moshkovich, D. Aurbach, *J. Electroanal. Chem*., 1999, **466**, 203–217.

52. I. Shterenberg, M. Salama, Y. Gofer, D. Aurbach, *Langmuir*, 2017, **33**, 9472–9478.

53. C. Liao, N. Sa, B. Key, A. K. Burrell, L. Cheng, L. A. Curtiss, J. T. Vaughey, J.-J. Woo, L. Hu, B. Pan, Z. Zhang, *J. Mater. Chem. A*, 2015, **3**, 6082–6087.

54. I. Shterenberg, M. Salama, H. D. Yoo, Y. Gofer, J.-B. Park, Y.-K. Sun, D. Aurbach, *J. Electrochem.*

Soc., 2015, **162**, A7118–A7128.

55. Y. Cheng, R. M. Stolley, K. S. Han, Y. Shao, B. W. Arey, N. M. Washton, K. T. Mueller, M. L. Helm, V. L. Sprenkle, J. Liua, G. Li, *Phys. Chem. Chem. Phys.,* 2015, **17**, 13307–13314.

56. N. Sa, B. Pan, A. S.-Shah, A. A. Hubaud, J. T. Vaughey, L. A. Baker, C. Liao, A. K. Burrell, *ACS Appl. Mater. Interfaces*, 2016, **8**, 16002–16008.

57. M. Kerner, N. Plylahan, J. Scheers, P. Johansson, *Phys. Chem. Chem. Phys.,* 2015, **17**, 19569–19581.

58. D. Aurbach, I. Weissman, A. Zaban, O. Chusid, *Electrochim. Acta*, 1994, **39**, 51–71.

59. P. C. Howlett, E. I. Izgorodina, M. Forsyth, D. R. MacFarlane, *Z. Phys. Chem*., 2006, **220**, 1483–1498.

60. R. Miao, J. Yang, X. Feng, H. Jia, J. Wang, Y. Nuli, *J. Power Sources*, 2014, **271**, 291–297.

61. M. Kar, Z. Ma, L. M. Azofra, K. Chen, M. Forsyth, D. R. MacFarlane, *Chem. Commun.,* 2016, **52**, 4033–4036.

62. G. G. Eshetu, S. Grugeon, G. Gachot, D. Mathiron, M. Armand, S. Laruelle, *Electrochim. Acta*, 2013, **102**, 133–141.

63. T. Watkins, D. A. Buttry, *J. Phys. Chem. B*, 2015, **119**, 7003–7014.

64. T. Mandai, K. Yoshida, S. Tsuzuki, R. Nozawa, H. Masu, K. Ueno, K. Dokko, M. Watanabe, *J. Phys. Chem. B*, 2015, **119**, 1523–1534.

65. J. Grondin, J.-L. Lasségues, M. Chami, L. Servant, D. Talaga, W. A. Henderson, *Phys. Chem. Chem. Phys*., 2004, **6**, 4260–4267.

66. P. Johansson, J. Grondin, J.-C. Lasségues, *J. Phys. Chem. A*, 2010, **114**, 10700–10705.

67. J. H Kim, Y. J. Oh, Y. C. Kang, *Carbon*, 2018, **128**, 125–133.

68. N. N. Rajput, X. Qu, N. Sa, A. K. Burrell, K. A. Persson, *J. Am. Chem. Soc*., 2015, **137**, 3411–3420.

69. M. Hattori, K. Yamamoto, M. Matsui, K. Nakanishi, T. Mandai, A. Choudhary, Y. Tateyama, K. Sodeyama, T. Uchiyama, Y. Orikasa, Y. Tamenori, T. Takeguchi, K. Kanamura, Y. Uchimoto, *J. Phys. Chem. C*, 2018, **122**, 25204−25210.

70. M. Herstedt, M. Smirnov, P. Johansson, M. Chami, J. Grondin, L. Servant, J. C. Lasségues, *J. Raman Spectrosc*., 2005, **36**, 762–770.

71. T. Mandai, K. Dokko, M. Watanabe, *Chem. Rec.*, 2018, **18**, 1–16.

72. M. Salama, I. Shterenberg, L. J. W. Shimon, K. K.-Adamsky, M. Afri, Y. Gofer, D. Aurbach, *J. Phys. Chem. C*, 2017, **121**, 24909−24918.

73. S.-J. Kang, S.-C. Lim, H. Kim, J. W. Heo, S. Hwang, M. Jang, D. Yang, S.-T. Hong, H. Lee, *Chem. Mater*., 2017, **29**, 3174−3180.

74. A. Haas, C. Klare, P. Betz, J. Bruckmann, C. Kruger, Y.-H. Tsay, F. Aubke, *Inorg. Chem*., 1996, **35**, 1918−1925.

75. G. Veryasov, K. Matsumoto, R. Hagiwara, *Dalton Trans*., 2016, **45**, 2810–2813.

76. G. Veryasov, U. Harinaga, K. Matsumoto, R. Hagiwara, *Eur. J. Inorg. Chem.,* 2017, 1087−1099

77. M. Steichen, N. R. Brooks, L. V. Meervelt, J. Fransaer, K. Binnemans, *Dalton Trans*., 2014, **43**, 12329–12341.

78. S. Schaltin, N. R. Brooks, J. Sniekers, L. V. Meervelt, K. Binnemans, J. Fransaer, *Chem. Commun.,* 2014, **50**, 10248–10250.

79. S. Schaltin, N. R. Brooks, J. Sniekers, D. Depuydt, L. V. Meervelt, K. Binnemans, J. Fransaer, *Phys. Chem. Chem. Phys.,* 2013, **15**, 18934–18943.

80. T. Mandai, P. Johansson, *J. Phys. Chem. C*, 2016, **120**, 21285–21292.

81. A. M.-Abbassi, M. Skripkin, M. Kritikos, I. Persson, J. Mink, M. Sandström, *Dalton Trans.,* 2003, 1746–1753.

82. E. G. Gumbris, E. V. Peresypkina, A. V. Virovets, and T. G. Cherkasova, *Rus. J. Inorg. Chem.,* 2012, 57, 337−342.

83. D. Brouillette, G. Perron, J. E. Desnoyers, *J. Sol. Chem*., 1998, **27**, 151–182.

84. L. Johnson, C. Li, Z. Liu, Y. Chen, S. A. Freunberger, P. C. Ashok, B. B. Praveen, K. Dholakia, J.-M. Tarascon, P. G. Bruce, *Nat. Chem*., 2014, **6**, 1091–1099.

85. N. N. Rajput, T. J. Seguin, B. M. Wood, X. Qu, K. A. Persson, *Top Curr. Chem*., 2018, **376**, 79–124.

Table of Contents

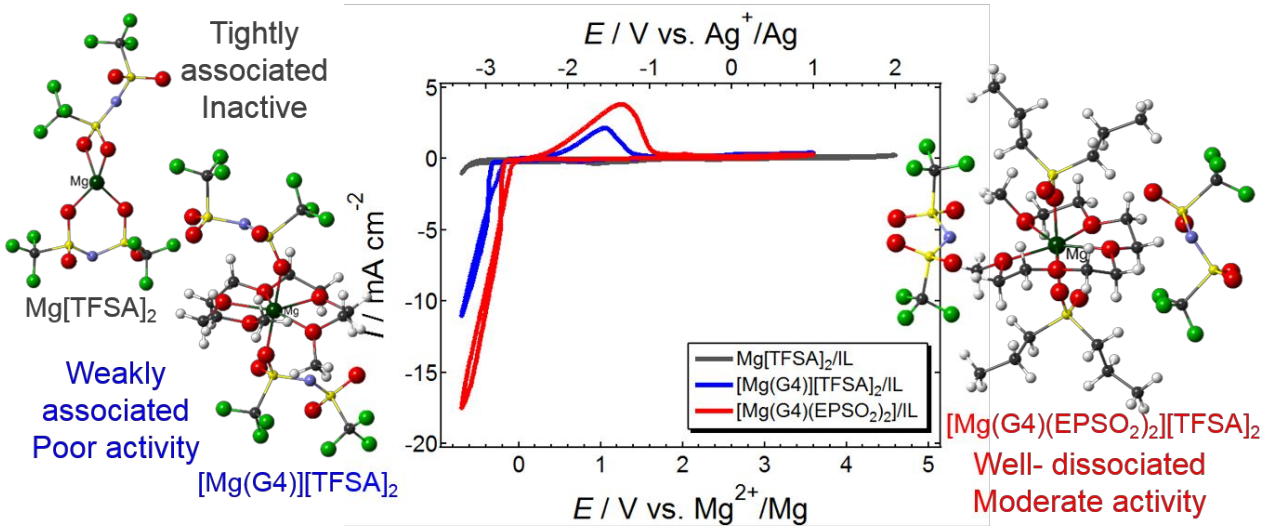

Systematic structural and electrochemical studies on the $Mg[TFSA]_2$-based electrolytes revealed that the coordination state of $[TFSA]^-$ predominates the electrochemical magnesium deposition/dissolution activity.